

Microstructure and texture evolution during severe plastic deformation of CrMnFeCoNi high-entropy alloy

W Skrotzki¹, A Pukenas¹, B Joni², E Odor^{2,3}, T Ungar^{2,3}, A Hohenwarter⁴,
R Pippan⁴, E P George^{5,6}

¹ Institut für Strukturphysik, Technische Universität Dresden, D-01062 Dresden, Germany

² Department of Materials Physics, Eötvös University, H-1117 Budapest, Hungary

³ Materials Performance Centre, School of Materials, The University of Manchester, Manchester M13 9PL, UK

⁴ Department of Materials Physics, Montanuniversität Leoben, A-8700 Leoben, Austria

⁵ Materials Science and Technology Division, Oak Ridge National Laboratory, Oak Ridge, TN 37831, USA

⁶ Department of Materials Science and Engineering, University of Tennessee, Knoxville, TN 37996, USA

werner.skrotzki@tu-dresden.de

Abstract. An equiatomic high-entropy alloy CrMnFeCoNi was severely deformed at room temperature by high pressure torsion up to shear strains of about 170. Its microstructure and texture were analyzed by X-ray diffraction (X-ray line profile analysis and X-ray microdiffraction, respectively). It is shown that at a shear strain of about 20 a steady state domain/grain size of 24 nm and a dislocation density of $3 \times 10^{16} \text{ m}^{-2}$ is reached, while the twin density goes over a maximum of 2% at this strain. The texture developed is typical for sheared face-centred cubic metals, but it is extremely weak. The results are discussed in terms of the mechanisms of deformation, including dislocation slip, twinning and grain boundary sliding.

1. Introduction

High entropy alloys (HEAs) represent a new class of single-phase multi-element (≥ 5) solid solution alloys with near-equiatomic concentrations of the individual elements [1]. In some cases, due to the large number of constituent elements the contribution of configurational entropy to the Gibbs free energy is high enough to suppress compound formation and phase separation. Among the wide variety of reported HEAs the most thoroughly investigated alloy is the quinary equiatomic face-centred cubic (FCC) HEA CrMnFeCoNi [2]. This alloy is stable as a single-phase solid solution at high temperatures [3], but decomposes into several different metallic and intermetallic phases at intermediate temperatures [4 - 6]. In the solid-solution state it exhibits certain noteworthy mechanical properties, including simultaneous strength and ductility increase with decreasing temperature [7] leading to outstanding fracture toughness at cryogenic temperatures [8].



To unravel the deformation mechanisms of these advanced alloys numerous investigations of microstructure and texture have been carried out on polycrystalline samples deformed in tension [9 - 11], and after swaging [12], rolling [13] and high pressure torsion (HPT) [5]. It is found that at room temperature and below, above a certain stress (equivalently strain) in addition to dislocation slip mechanical twinning contributes to deformation. Twinning is more pronounced at cryogenic temperatures. There is texture formation during deformation, but its intensity is quite low. The observed dislocation dissociation and texture are typical of medium stacking fault energy (SFE) metals and alloys.

The present paper extends recent work initiated by three of the present authors on CrMnFeCoNi HEA processed by HPT [5]. Here a detailed study is conducted of microstructure and texture evolution during severe plastic deformation.

2. Experimental

The CrMnFeCoNi HEA was synthesized from high-purity elements (> 99.9 wt.%) by arc melting and drop casting under pure argon atmosphere into cylindrical molds (diameter: 25.4 mm, length: 127 mm). The drop-cast ingots were encapsulated in evacuated quartz ampules and homogenized for 48 h at 1200°C. Discs with a radius $r = 4$ mm and an initial thickness $t_i \approx 0.8$ mm were cut from the cast and homogenized ingots and deformed by HPT [14]. During HPT the shear strain along the radius is approximately given by $\gamma = 2\pi n / \langle t \rangle$, where n is the number of rotations (Rot n) and $\langle t \rangle = (t_i + t_f)/2$ with t_f = final thickness. With this approximation the maximum error in shear strain is less than 15%. HPT was conducted at room temperature (RT) at a nominal speed of 0.2 rotations/min yielding a maximum initial shear strain rate of 10^{-1} s^{-1} at the outer radius. The initial grain size was several hundred micrometers, while the saturation microstructure after HPT as analysed by transmission electron microscopy was estimated to consist of grains with a size of about 50 nm. During HPT the alloy did not decompose as checked by 3D atom probe tomography [5].

To further investigate the microstructure, X-ray diffraction measurements were carried out in a special high-resolution diffractometer dedicated to line-profile-analysis with a plane Ge (220) primary monochromator operated at the Cu $K\alpha$ fine focus rotating copper anode (Rigaku, RA-MultiMax9) at 40 kV and 100 mA [15]. The distance between the source and the monochromator is 240 mm and a slit of about 160 μm is placed before the monochromator, 200 mm from the X-ray source. In this configuration the $K\alpha_1$ and $K\alpha_2$ components arrive at the Ge (220) crystal with a large enough separation to allow the $K\alpha_2$ component to be cut off by the 160 μm wide slit. The Cu $K\alpha_1$ beam has a size of about 0.2×1.5 mm on the specimen surface. The scattered radiation is registered by two curved imaging plates (IP) with a linear spatial resolution of 50 μm . The IPs are placed at distances of 200 mm from the specimen covering the angular range $30^\circ \leq 2\theta \leq 153^\circ$. The distances between the specimen and detector are selected such that the instrumental effect is always less than 10% of the physical broadening. The diffraction geometry is of parallel-beam type; therefore the specimen does not have to be moved and sufficient angular resolution is achieved over the entire angular range of measurement. The diffraction patterns are obtained by integrating the intensity distributions along the corresponding Debye-Scherrer arcs on the IPs. Only the central parts of the arcs are used for the integration where the curvature does not affect line broadening. The X-ray beam is positioned on the specimen surface by using a low depth-resolution microscope coupled to a TV-screen. The measurements are done at about the centre, half radius and close to the edge of the samples, i.e. at positions where the shear strains are different.

The line profiles are evaluated by using the convolutional multiple whole profile (CMWP) procedure [16]. The measured diffraction pattern is matched by the theoretically calculated and convoluted profile functions accounting for the effects of size, distortion, planar defects and instrumental effects, while the background is determined separately. Because of the double-crystal high resolution diffractometer, described above, the instrumental effect is neglected. The parameter values that characterize the substructure, namely the area average crystallite (subgrain) size $\langle x \rangle_{\text{area}}$,

dislocation density ρ , dislocation character q (edge versus screw), dislocation arrangement parameter $M = R_e \sqrt{\rho}$ (R_e = effective outer cut-off radius of dislocations), twin density β (number of twin boundary planes within hundred lattice planes parallel to the twin boundary) and average distance between adjacent twin boundaries $d_{Tw} = 100 d_{\{111\}}/\beta$ are obtained by using the CMWP method.

In order to resolve the local texture of the deformed discs along the radial direction, i.e. as a function of increasing shear strain from the middle to the edge of the disc, two-dimensional X-ray micro diffraction was performed using the system D8 Discover (BRUKER AXS GmbH) equipped with an Euler cradle including x-y-z-stage, a laser-video adjustment system, a low-power micro-focus X-ray tube I μ S (spot size about 100 μ m) and a two-dimensional detector VÅNTEC 2000. The intensities of the measured Debye-Scherrer rings were integrated along their curvature to calculate the pole figures (200, 220, 111) on a 5°×5° grid. For calculation of the orientation distribution function (ODF) with these pole figures Multex 3 [17] and LaboTex software [18] were used. The Euler angles given are in the Bunge notation [19] with crystal and sample reference systems defined as x ||shear direction, y ||shear plane normal and z ||transverse direction yielding an ODF representation appropriate for simple shear [20]. The textures are represented by $\varphi_2=45^\circ$ ODF sections, which for FCC metals contain all major shear components.

3. Results and Discussion

Typical diffraction patterns of HPT deformed CrMnFeCoNi HEA specimens are shown in Fig. 1. The quality of the fitting procedure by using the CMWP method can be assessed by the measured (open circles) and the fitted (red line) diffraction patterns.

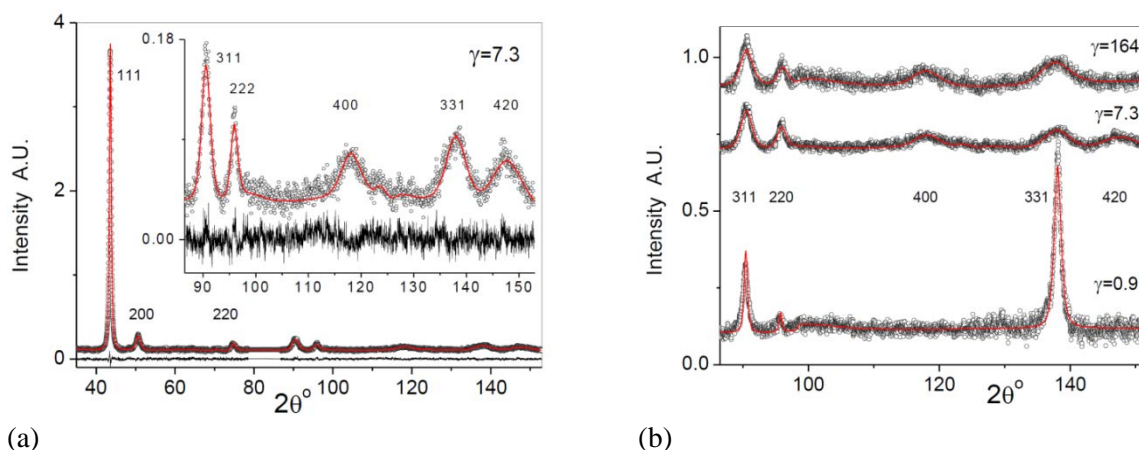


Figure 1. Typical diffraction patterns of HPT deformed CrMnFeCoNi HEA specimens. (a) Measured (open circles) and CMWP calculated (red lines) patterns for shear strain $\gamma = 7.3$ are shown using logarithmic intensity scales. The inset is the enlarged part of the pattern at higher diffraction angles. (b) Comparison of diffraction patterns after different shear strains: $\gamma = 0.9$, 7.3 and 164.

The results of the CMWP analysis show that during HPT of CrMnFeCoNi HEA a very fast refinement of the microstructure takes place. The crystallite size ($\langle x \rangle_{area}$) reaches a very low steady state value of 24 nm after a shear strain of about 20 (Fig. 2a). Simultaneously, the dislocation density saturates at $3 \times 10^{16} \text{ m}^{-2}$ (Fig. 2b). While the dislocation character q changes from near edge- ($q_{edge} = 1.4$) to near screw-type ($q_{screw} = 2.4$) and then slightly decreases again (Fig. 2c), the dipole character M is quite weak ($M > 1$) and saturates at about 6 (Fig. 2d). The twin density has a maximum of 2% at $\gamma \approx 20$ (Fig. 2e) leading to a mean twin separation distance d_{Tw} smaller than $\langle x \rangle_{area}$ for $10 < \gamma < 60$ (Fig. 2f).

The texture observed after HPT is the typical shear texture observed in FCC metals and alloys. Because of the initial coarse grain structure the texture measured by microdiffraction is statistically

reliable only after a shear strain of about 5. As shown in Fig. 3a the texture of CrMnFeCoNi HEA is quite weak (below 2.5 mrd). The main texture components developed by dislocation slip and mechanical twinning are $\{111\}\langle 112 \rangle$ (A_1^*/A_2^*) and $\{112\}\langle 110 \rangle$ (B/\bar{B}), with (B/\bar{B}) dominating (Fig. 3b). With increasing twinning activity the volume fraction of these components decreases. When twinning ceases texture intensity initially increases but then decreases again at high shear strains.

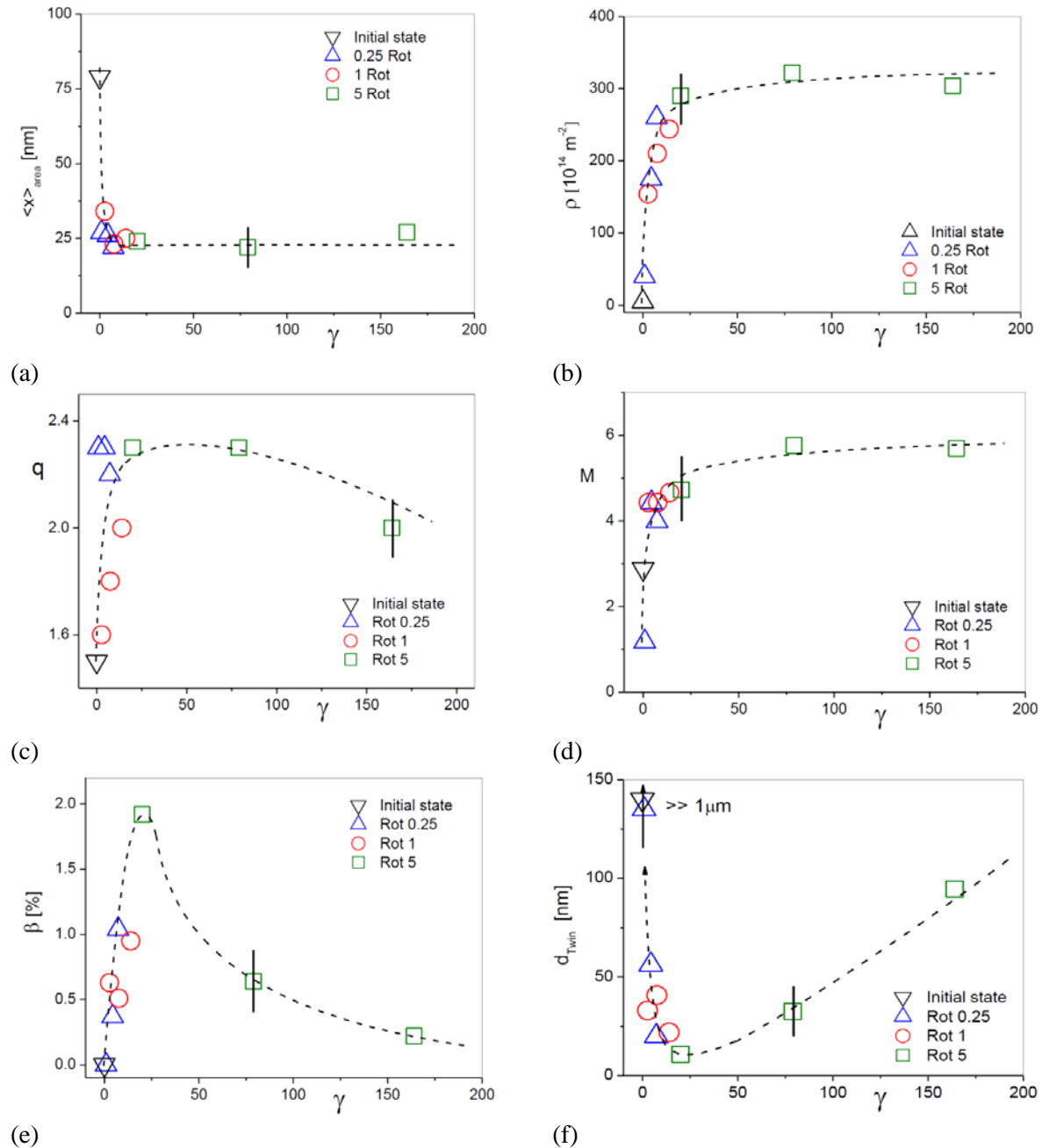


Figure 2. (a) Grain size $\langle x_{\text{area}} \rangle$, (b) dislocation density ρ , (c) dislocation character q , (d) dislocation arrangement parameter M , (e) twin density β and (f) average distance between adjacent twin boundaries d_{Tw} versus shear strain γ .

The strong grain refinement is correlated to the high mechanical twinning activity in the medium SFE ($\leq 30 \text{ mJm}^{-2}$ [21 - 23]) alloy [5, 10]. Based on TEM investigations a mechanism of fast grain

refinement via primary and secondary twinning has been proposed by Wang et al. [24] for brass. Primary twins by accumulation of a high density of dislocations evolve into curved high angle grain boundaries from which secondary twins are emitted. The emission of secondary twins further refines the grains and transforms the elongated grains into equiaxed nanograins. At a certain shear strain twinning ceases, may be because grain boundary sliding takes over as the deformation mechanism. A supporting indication of this is the further randomization of texture. The generally low texture strength may be also caused by twinning. Twinning may have led to the almost equal intensities of the twinning related A_1^* and A_2^* shear components. Texture simulations to check this are planned.

The medium SFE of this alloy leads to widely dissociated dislocations (screws: $\cong 4$ nm, edges: $\cong 6$ nm) [21]. After relatively low compressive strains at 77 K, long smoothly curved dislocations having mixed character are seen on the $\{111\}$ planes suggesting that the mobilities of edge and screw dislocations are not significantly different [21]. Here we find that at RT the dislocation character tends to become more screw-like with increasing shear strain, peaking at a value of $q \approx 2.3$ at a shear strain $\gamma \approx 25$ and then decreasing thereafter to $q \approx 2$ at $\gamma \approx 170$. It is somewhat surprising that the dipole character of dislocations observed is low ($q > 1$) and decreases further with increasing dislocation density. This may be caused by the wide dislocation dissociation suppressing edge dislocation climb and screw dislocation cross slip.

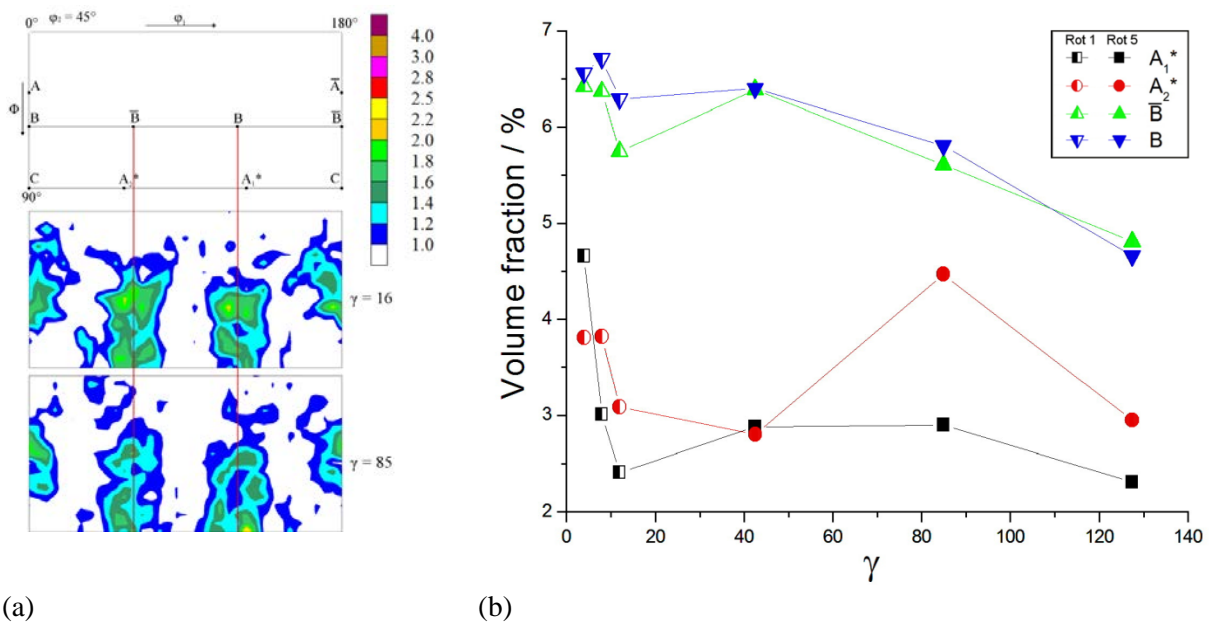


Figure 3. (a) Texture represented as $\phi_2 = 45^\circ$ ODF sections at different shear strains γ . Intensities are given in multiples of a random orientation distribution. The key figure shows the main texture components that develop during simple shear of FCC metals. (b) Volume fraction of texture components (15° FWHM) versus shear strain γ .

The brass-type texture in shear with strong B/\bar{B} components agrees with results of texture simulations on HPT samples of nanocrystalline Pd-10at.%Au alloy [25] and rolling of nanocrystalline Ni-18.7 at.%Fe alloy [26]. These simulations strongly suggest that nanoplasticity is determined by slip of partial dislocations emitted from the grain boundaries also leading to twinning. Recent simulations also show that grain boundary sliding leads to randomization of the texture while maintaining the texture signature [27].

4. Conclusions

- (1) HPT leads to strong grain refinement of the CrMnFeCoNi HEA. This may be caused by severe mechanical twinning in addition to dislocation slip.

- (2) Correlated with the low grain size is a high remnant dislocation density. These dislocations are predominantly screw-type and show a weak dipole character due to a wide dissociation into Shockley partials.
- (3) The weak texture is a dominant brass-type shear texture indicating the deformation during SPD occurs mainly by partial dislocation slip accompanied by twinning and grain boundary sliding.

Acknowledgments

Funding of this work (A.H. and R.P.) has been provided by the European Research Council under ERC Grant Agreement No. 340185 USMS and by the Austrian Science Fund (FWF) in the framework of research project P26729-N19. E.P.G is sponsored by the U.S. Department of Energy, Office of Science, Basic Energy Sciences, Materials Sciences and Engineering Division.

References

- [1] Yeh J W, Chen S K, Lin S J, Gan J Y, Chin T S, Shun T T, Tsau C H and Chang S Y 2004 *Adv Eng Mater* **6** 299
- [2] Cantor B, Chang I T H, Knight P and Vincent A J B 2004 *Mater Sci Eng A* **375-377** 213
- [3] Otto F, Yang Y, Bei H and George E P 2013 *Acta Mater* **61** 2628
- [4] Otto F, Dlouhy A, Pradeep K G, Kubenova M, Raabe D, Eggeler G and George E P 2016 *Acta Mater* **112** 40
- [5] Schuh B, Mendez-Martin F, Völker B, George E P, Clemens H, Pippan, R and Hohenwarter A 2015 *Acta Mater* **96** 258
- [6] Pickering E J, Munoz-Moreno R, Stone H J and Jones, N G 2016 *Scripta Mater* **113** 106
- [7] Gali A and George E P 2013 *Intermetallics* **39** 74
- [8] Gludovatz B, Hohenwarter A, Catoor D, Chang E H, George E P and Ritchie R O 2014 *Science* **345** 1153
- [9] Otto F, Dlouhy A, Somsen Ch, Bei H, Eggeler G and George E P 2013 *Acta Mater* **61** 5743
- [10] Stepanov N, Tikhonovsky M, Yurchenko N, Zyabkin D, Klimova M, Zharebtsov S, Efimov A and Salishchev G 2015 *Intermetallics* **59** 8
- [11] Laplanche G, Kostka A, Horst O M, Eggeler G and George E P 2016 *Acta Mater* **118** 152
- [12] Laplanche G, Horst O, Otto F, Eggeler G and George E P 2015 *J Alloys Comp* **647** 548
- [13] Sathiaraj G D and Bhattacharjee P P 2015 *J Alloys Comp* **647** 82
- [14] Pippan R, Scheriau S, Hohenwarter A and Hafok M 2008 *Mater Sci Forum* **584-586** 16
- [15] Ungar T, Ott S, Sanders P G, Borbely A and Weertman J R 1998 *Acta Mater* **10** 3693
- [16] Balogh L, Ribarik G and Ungar T 2006 *J Appl Phys* **100** 023512
- [17] Multex Manual, Multex 3, 2008, Bruker AXS GmbH (Karlsruhe, Germany).
- [18] Pawlik K 1986 *Phys Stat Sol (b)* **134** 477
- [19] Bunge H-J 1965 *Z Metallkde* **56** 872
- [20] Tóth L S and Molinari A 1994 *Acta Metall Mater* **42** 2459
- [21] Okamoto N L, Fujimoto S, Kambara Y, Kawamura M, Chen Z M T, Matsunshita H, Tanaka K, Inui H and George E P 2016 *Sci Reports* DOI: 10.1038/srep35836
- [22] Yeh J W 2015 *JOM* **67** 2254
- [23] Huang S, Li W, Lu S, Tian F, Shen J, Holmström E and Vitos L 2015 *Scripta Mater* **108** 44
- [24] Wang Y B, Liao, X Z, Zhao Y H, Lavernia E J, Ringer S P, Horita Z, Langdon T G, Langdon T G and Zhu Y T 2010 *Mater Sci Eng A* **527** 4959
- [25] Skrotzki W, Eschke A, Joni B, Ungar T, Toth L S, Ivanisenko Yu and Kurmanaeva L 2013 *Acta Mater* **61** 72
- [26] Li L, Ungar T, Toth L S, Skrotzki W, Wang J D, Ren J, Choo H, Fogarassy Z, Zhou X Z and Liaw P K 2016 *Metall Mat Trans A* **47** 6632
- [27] Zhao Y, Toth L S, Massion R and Skrotzki W 2017 *Adv Eng Mater*, submitted